Electronic Suplementary Information

for

Two birds with one stone: colorimetric and photothermal dual-mode biosensor based on CoOOH nanorings for detecting *β*-galactosidase activity and *Escherichia coli*†

Yong Qiong Wang[a], Jia Hui Liu[b], De Yan Li[a], Jin Zhang[a], Long Huang[a], Jian Mei Yang[a], and Tong Yang*[,a]

[a] Yunnan Key Laboratory of Modern Separation Analysis and Substance Transformation, College of Chemistry and Chemical Engineering, Yunnan Normal University, Kunming 650500, Yunnan Province, P. R. China.
[b] Institute of Biomedical Engineering, Kunming Medical University, Kunming 650500, P. R. China.

*Corresponding E-mails: yangtong@ynnu.edu.cn, yt09132149@163.com (T. Yang)

Table of Contents

Experimental Section

Reagents and Materials. Cetyltrimethylammonium bromide (CTAB), cetyltrimethylammonium chloride (CTAC), and sodium borohydride ($NaBH_4$, 99%) were purchased from Tianjin Fuchen Chemical Reagent Co., Ltd. (Tianjin, China). Ascorbic acid (AA) was provided by Roen Technology Co., Ltd. (Beijing, China). α-galactosidase (α-Gal), and β-galactosidase (β-Gal) were purchased from Solebaum Biotechnology (Beijing, China). $HAuCl_4 \cdot 3H_2O$, benzyldimethylhexadecylammonium chloride (HDBAC), and *p*-aminophenyl-β-D-galactopyranoside (PAPG) were purchased from Aladdin Chemicals (Shanghai, China). Bacterial Protein Extraction Kits were bought from Shanghai Sangon Biological Engineering Technology and Services Co., Ltd. (Shanghai, China). Microbial β-galactosidase (β-gal) ELISA kit was acquired from Jiangsu Enzyme Immunity Industrial Co., Ltd. (Jiangsu, China). BL21(DE3) cell receptor state was purchased from Beijing BioMed Biotechnology Co., Ltd. (Beijing, China). Tryptone Soy Broth (TSB), and 90 mm disposable bacterial culture dish and BS-PS-A disposable plastic applicator stick were purchased from Haibo Biotechnology Co., Ltd. (Qingdao, China), and Labgic Technology Co., Ltd.. (Biosharp, Hefei, China).

Apparatuses. Transmission electron microscopy (TEM, JEM2100, Tokyo, Japan) and field emission scanning electron microscopy (SEM, SU8020, Hitachi, Japan) were used to study the morphological characterization of Au NBPs and CoOOH respectively. The Thermostatic Mixer were applied to incubate the reaction mixed solution (Eppendorf/ThermoMix C). UV-visible spectral measurements were performed using a UV-2700 spectrophotometer (Shimadzu Corporation, Japan) to record the LSPR absorption peaks of Au NBPs. X-ray diffraction (XRD) was measured using Ultima IV diffractometer (Nippon science Co., Japan) for characterization of CoOOH NRs. Full spectral analysis of CoOOH by X-ray photoelectron spectroscopy (XPS, Thermo Fisher Scientific). Electron spin resonance spectrum (Bruker, Germany) was used for the characterization of reactive oxygen species (ROS). Cell phone temperature measurement thermal imaging camera was purchased from Hangzhou Hikmicro Sensing Technology Co., Ltd. (Hangzhou, China) for photothermal detection.

Synthesis of Au NBPs. The synthesis and purification of Au NBPs are consistent with the steps of our previously reported work.[1]

Preparation of CoOOH Nanorings. The CoOOH NRs were prepared with minor modification based on the experimental steps in previously reported work.[2] At first, $CoCl_2$ solution (50 mL, 10 mM) was mixed with NaOH solution (1.5 mL, 1.0 M), followed by sonication for 5 minutes. The mixture was then centrifuged at 7800 rpm for 20 minutes. Second, the precipitate was dispersed in 50 mL of deionized water (DIW), and 2.5 mL of NaClO (0.9 M) was added. The mixture was treated with ultrasound for 20 minutes, and then centrifuged at 7800 rpm for 10 minutes. The resulting precipitate was washed three times with deionized water. Finally, it was dried overnight in a vacuum drying oven at 60 ℃.

CoOOH-based colorimetric analysis and photothermal analysis of β-galactosidase (β-Gal). Different concentrations of β-Gal standard solutions (40 μL) respectively reacted with 4-aminophenyl-β-D-galactopyranoside (PAPG, 4 mM, 50 μL). After incubation for 30 min at 37 ºC, the HAc-NaAc buffer (0.02

M, pH 4.5, 150 μL), CoOOH (0.8 mg/mL, 10 μL) were added and reacted for 10 min, followed by KI (50 μL 12 mM) and Au NBPs (100 μL) in the above reaction solution and incubated at 37 °C for 20 min. The final concentrations of β-Gal standard solutions are 0, 5.0, 10.0, 20.0, 50.0, 100.0, 200.0, 500.0, 1000.0, 2000.0, 3000.0, 4000.0, 5000.0 U/L.

In addition, the chromogenic solution was irradiated with a 1 W near-infrared laser at 808 nm for 3 min, and the temperature change before and after the reaction was measured with a mobile phone thermal imaging camera. Finally, the concentration of β-Gal could be detected quantitatively. The construction of detection system was displayed in Electronic Supplementary Information (Fig. S1). The distance between laser and samples is 5 cm. The distance between the photothermal imaging camera USB and samples is about 3 cm to obtain the suitable imaging area. The

Culture and Counting of Bacteria. *E. coli* BL21 was cultivated in TSB medium and incubated overnight in a shake bed at 37 °C, 220 rpm. Concurrently, a plate count was employed to quantify the bacteria. A 100 μL of diluted solution was uniformly smeared on the solid medium plates. The number of colonies of bacteria was counted by counting the number of colonies on the cultural dish. Ultimately, the concentration of the *E. coli* cells used in this experiment was worked out to be approximately 7.0×10^7 CFU/mL (The average value originated from plate counting in Fig. S2).

***β*-Gal-Mediated Multicolor and Photothermal Analysis of *E. coli*.** The overnight culture of *E. coli* BL21 was serially diluted with PBS solution, obtaining desired concentrations (2×10^2, 1×10^3, 2×10^3, 1×10^4, 2×10^4, 1×10^5, 2×10^5, 1×10^6, 2×10^6, 1×10^7, 2×10^7, and 3×10^7 CFU/mL). Then, *E. coli* was treated by using the Bacterial Protein Extraction Kit to ensure efficient lysis of *E. coli*. After lysis, the supernatants containing soluble proteins, enzymes including target β-Gal, and so on, is collected by centrifugation at 8000 rpm for 5 min at 4 °C by temperature-controlled centrifuge. Then, the collected supernatant can be used for colorimetric analysis to complete the analysis of *E. coli* samples by measuring β-Gal activity. The analysis steps are the same as the standard β-Gal analysis procedure.

Pretreatment of milk contaminated by *E. coli*. The sterile milk purchased from the local market. The milk samples were added *E. coli* by experimental operator. Then, the opened milk and contaminated milk was incubated in a shaker at 37 ℃ for 24 h, respectively. Pretreatment procedures were performed according to the instructions from the Bacterial Protein Extraction Kit. Detailedly, 8 mL of milk was taken in a 10 mL centrifuge tube and centrifuged at 8000 rpm for 10 min to collect the bacterial bodies. The supernatant (containing milk solution) was discarded, and the precipitate (containing *E. coli*) was washed with PBS buffer for a few times. After resuspending each 400 μL of bacterial precipitate containing 1× lysis buffer, 4 μL of PMSF and 8 μL of lysozyme were added sequentially, incubating the bacterial suspension at 37 °C for 30 min on a shaker. Then, add 20 μL of DNase/RNase was added in the mixtures, continuing to incubate the mixture on a shaker for 10 min at 37 °C. The mixtures were centrifuged in a refrigerated centrifuge at 4 °C for 30 min at 5000 rpm, removing the insoluble material from the precipitate. Finally, the protein supernatant was collected in a clean test tube for further use. All experiments were conducted triplicate or more.

Colorimetric and Photothermal Dual-Mode Analysis of *β*-Gal and *E. coli* in actual food samples. The ripe and fresh fruits including kiwis, oranges, and strawberries were bought from the local market. After twenty days of storage, the rot fruits were collected. Then, the orange, strawberry, and kiwi were peeled, and 15 grams of sarcocarp ground into a homogeneous mixture. The prepared fruit homogenate was

centrifuged (8,000 rpm, 10 min). The supernatant was collected and filtered to remove insoluble matter. Finally, after diluting the supernatant 5-fold with deionized water, the same steps are followed for colorimetric and photothermal analysis. The detection procedures of β-Gal were in accordance with the above procedures.

The sterile milks were purchased from the local market. To simulate actual *E. coli* growth, 8 mL of contaminated milk was incubated in a shaker at 37°C for 24 hours. Pretreatment procedure was then carried out according to the steps of the Bacterial Protein Extraction Kit, which was displayed in Supporting Information. The incubated bacterial samples were collected and subjected to chromogenic and photothermal analysis according to the method proposed in this study. Finally, the detection procedures of bacteria were in accordance with the above procedures. All experiments were conducted triplicate or more.

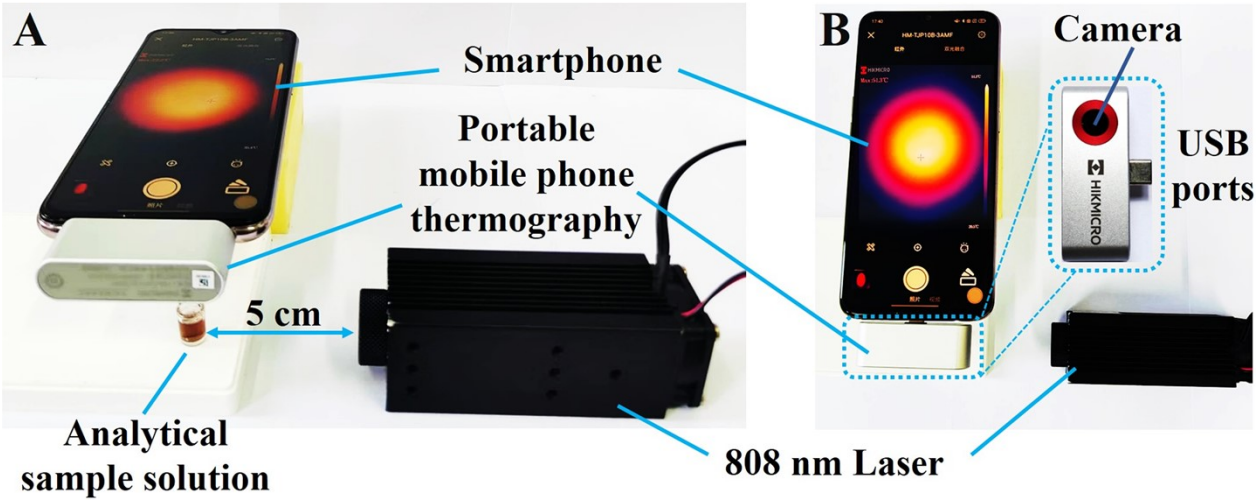

Fig. S1. Photograph of the portable photothermal detection. (A) Front view of photothermal detection. (B) Vertical view of photothermal detection.

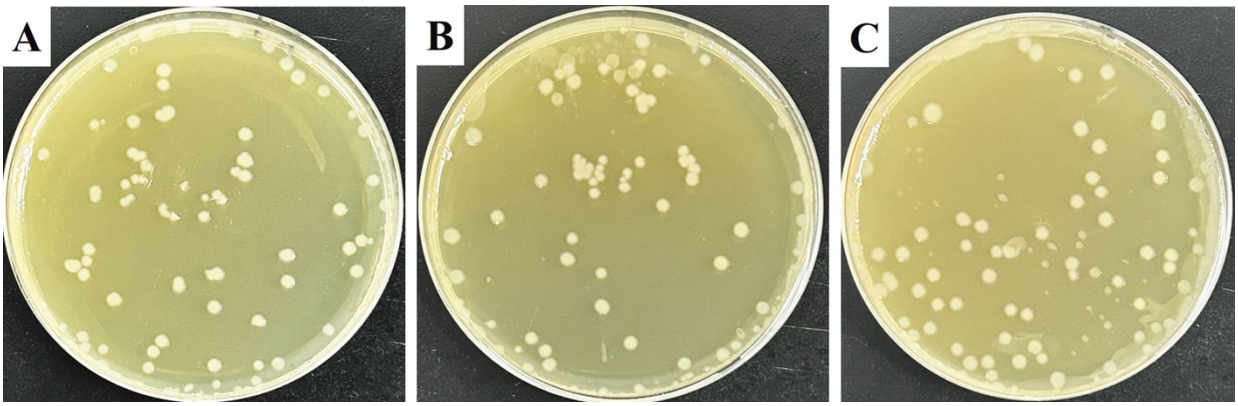

Fig. S2. The plate count of *E. coli*. (A), (B) and (C) are three groups of parallel samples.

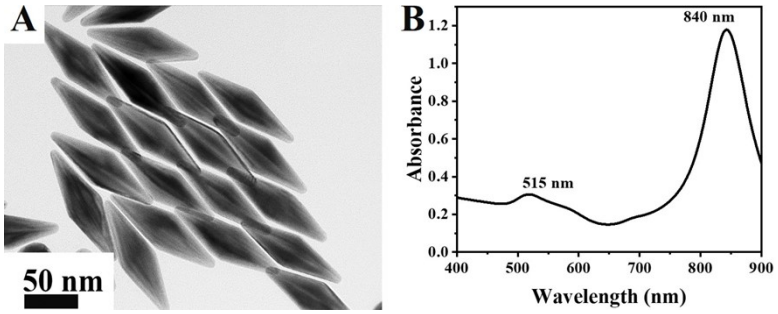

Fig. S3. Synthesis of Au NBPs. (A) TEM images of Au NBPs. (B) UV-Vis absorption spectrum of Au NBPs.

Note: In this work, Au NBPs with uniform bipyramids nanostructures (TEM image, Fig. S3A), were used as visual nanoplasmonic probes, whose horizontal and longitudinal LSPR absorption peaks located at ~515 nm and ~840 nm (Fig. S3B), respectively. The longitudinal LSPR absorption peak served as a signal output unit to detect *β*-Gal and *E. coli.*

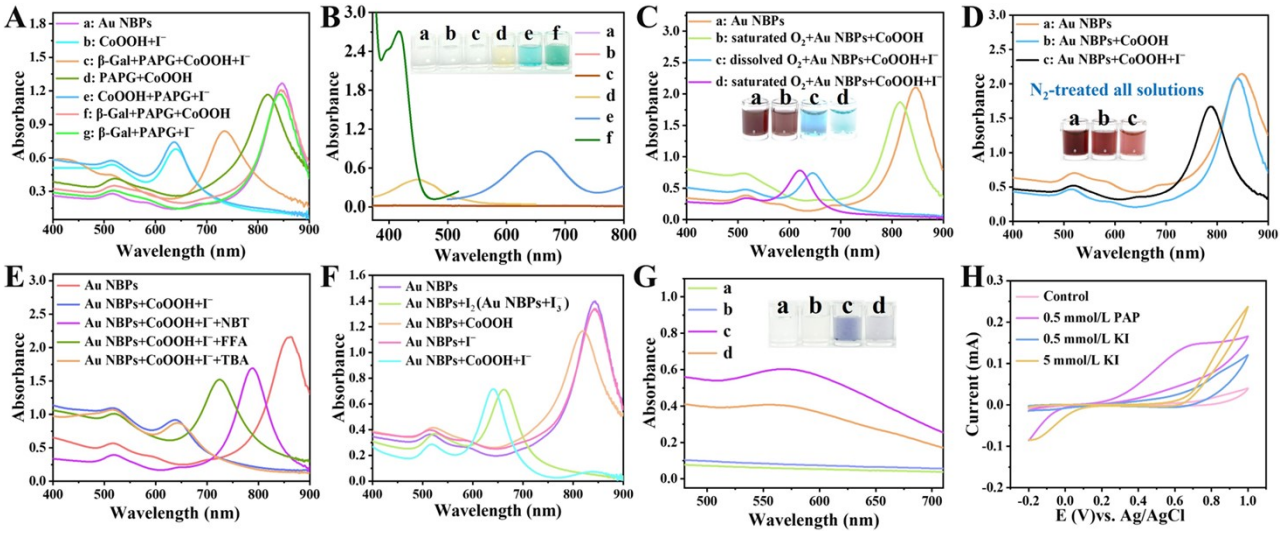

Fig. S4. Feasibility analysis and investigation of sensing mechanism. (A) Feasibility analysis for detecting *β*-Gal based on the CoOOH NRs by UV-Vis spectrum of AuNBPs in the different analytical solutions. (B) UV-Vis spectrum and colorimetric photograph of different chromogenic substrates (OPD, TMB, and ABTS) in the absence (a~c: control groups) and presence (d~f: experimental groups) of CoOOH. (C) Dissolved O_2 effect of CoOOH as oxidase-like mimics by UV-Vis spectrum of Au NBPs in different analytical systems. (D) Investigation of the oxidative properties of CoOOH toward oxidizing I^- under saturated N_2-treated solutions by UV-Vis spectrum of Au NBPs. (E) Investigations of main ROS toward etching Au NBPs by using nitro blue tetrazolium (NBT), furfuryl alcohol (FFA), and tert-butanol (TBA) as $O_2^{\bullet-}$, $^1O_2$, and $\bullet OH$ scavengers, respectively. (F) Etching effect investigations of I_2 toward Au NBPs in analytical systems. (G) Characteristic experiments of starch/I_2, UV-Vis spectrum of starch/I_2 in different situations: (a) CoOOH + I^-, (b) CoOOH+starch, (c) CoOOH+I^-+starch, (d) saturated N_2-treated CoOOH+I^-+starch. (H) CV curves of bare CoOOH (as control, without I^- and PAP), CoOOH+PAP (0.5 mM), CoOOH+I^- (0.5 mM, 5 mM).

Note: From Fig. S4H, there are no obvious oxidation and redox peaks of I^- in CV curves by using CoOOH as electrode materials, but the current signal increase with the increasing concentrations of I^-, testifying the weak oxidized capacity of CoOOH toward I^-. In comparison, the obvious PAP oxidation peak occurred at 0.714 V, indicating that PAP was more easily oxidized than I^- by CoOOH. Therefore, the existence of PAP as a reducing agent not only consumes ROS, but also reacts with CoOOH in analytical system, which can greatly reduce the generation of I^- into I_2 to slow down the corrosion of Au NBPs.

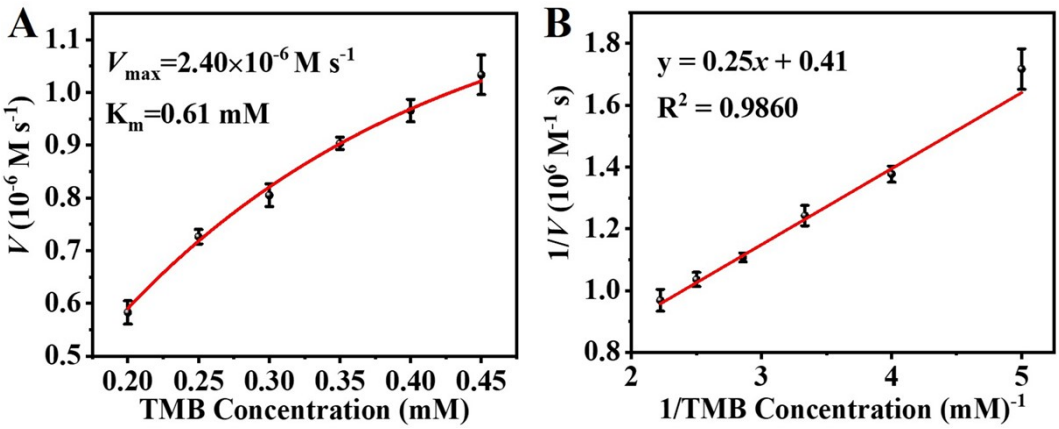

Fig. S5. Steady-state kinetics and Lineweaver-Burk reciprocal plots of CoOOH with oxidase-like activity using different concentrations of TMB as substrate (A and B).

Note: The steady-state kinetic constant K_m value of TMB was 0.61 mM by Michaelis-Menten curves (Fig. S5, ESI†), confirming that CoOOH as a week oxidase-like mimic exhibited a certain affinity toward TMB.

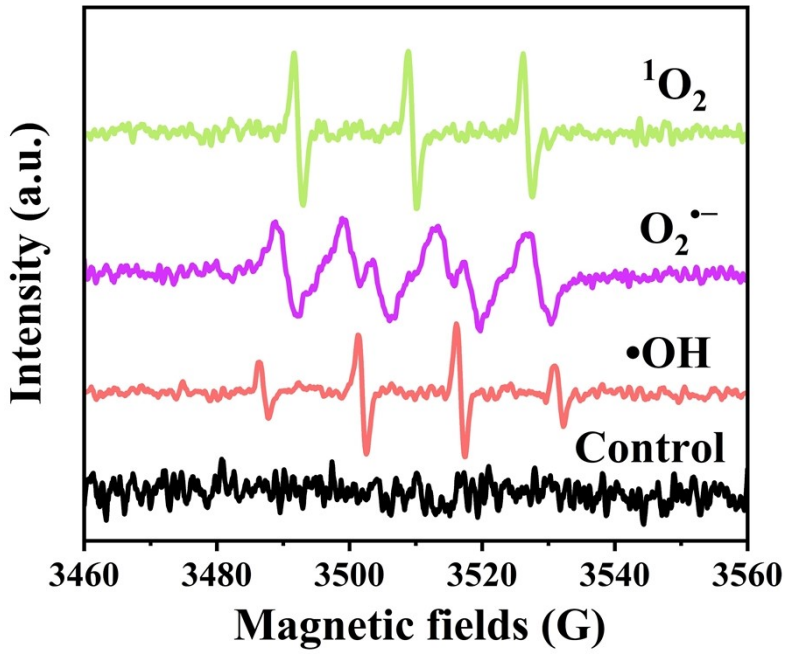

Fig. S6. EPR spectrum of $O_2^{\bullet-}$, $^1O_2$, and •OH using CoOOH as an oxidase-like mimic, respectively. (Control groups: without CoOOH NRs)

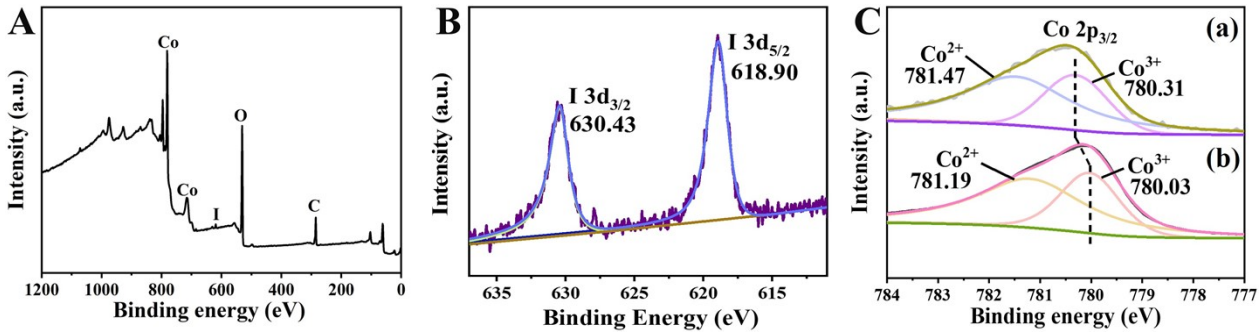

Fig. S7. (A) XPS fully scanned spectra of CoOOH nanorings after reacting with KI. (B) High-resolution XPS spectra of I 3d orbit of CoOOH nanorings after reacting with KI. (C) High-resolution XPS spectra of Co 2p orbit of (a) original CoOOH nanorings and (b) CoOOH nanorings after reacting with KI.

Note: The relevant XPS spectra of CoOOH NRs after reacting with KI were measured (Fig. S7). The featured peaks at 630.43 and 618.90 eV of I 3d orbital HR-XPS could vividly prove the existence of I_2 in accordance with the previous work.[3] The HR-XPS peaks of Co^{3+} and Co^{2+} in CoOOH NRs shift from high energy area to low energy area before and after reacting with KI, proving that the redox reaction between CoOOH and I^- led to the variation of redox couple ratio of Co^{3+}/Co^{2+} in CoOOH NRs.

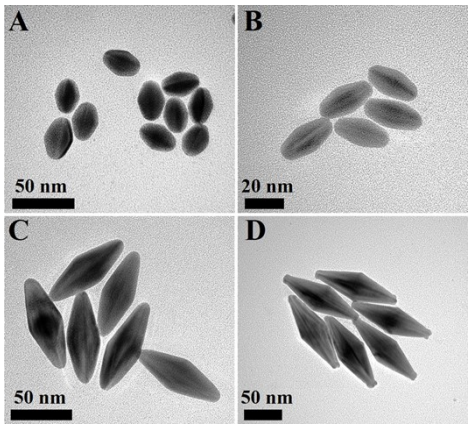

Fig. S8 TEM images of etched Au NBPs in analytical systems (PAPG + CoOOH + I^-) with different activities of *β*-Gal: (A) 1.0, (B) 5.0, (C) 50.0, and (D) 200.0 U/L, respectively.

Note: From the Fig. S8, with the increasing β-Gal activities, the morphological transformations of Au NBPs were presented from bipyramid, rice grain-like shape, to spherical shape. It was demonstrated that the introduction of β-Gal activities in analytical system could actually inhibit the corrosion of Au NBPs, which exhibited a certain feasibility for detecting β-Gal.

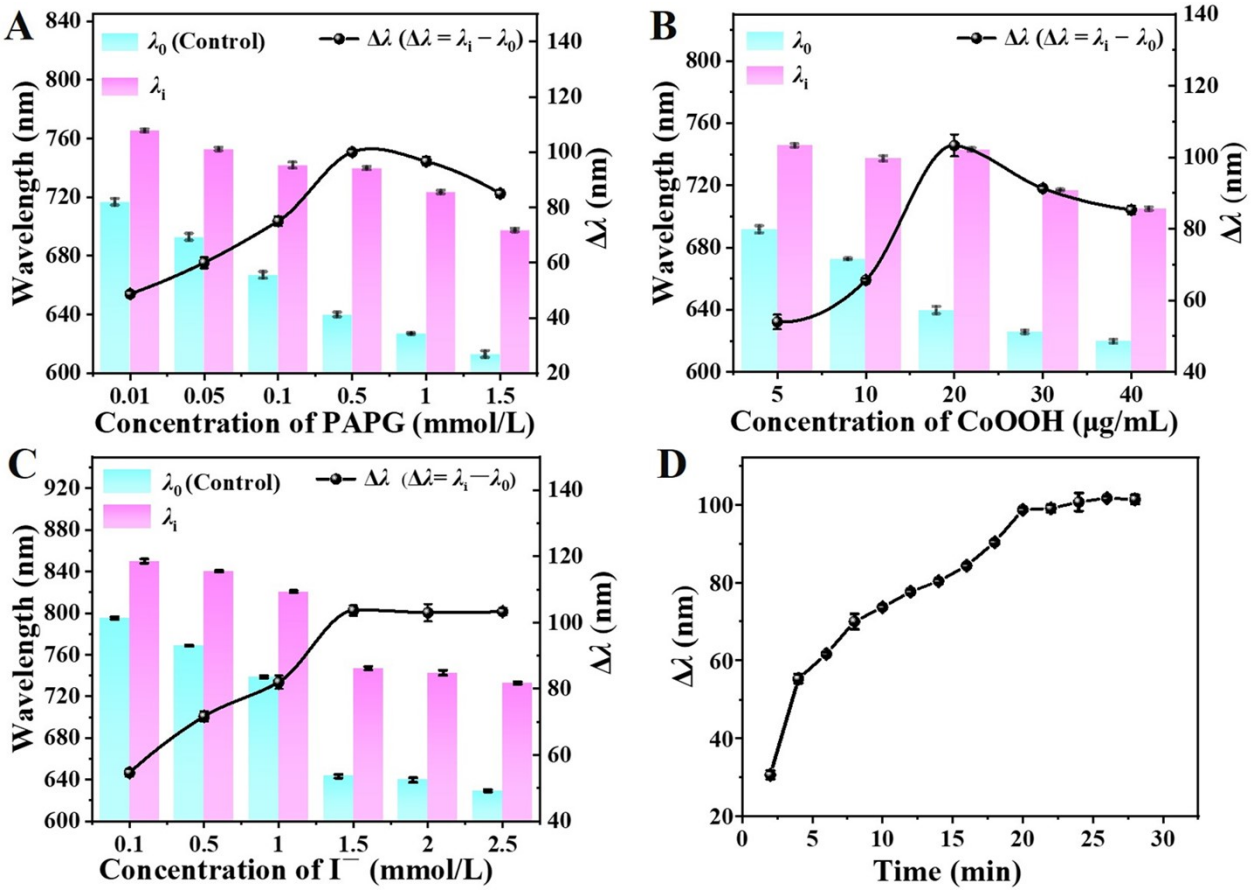

Fig. S9. Optimization of experimental conditions. The concentrations effect of (A) PAPG substrate, (B) CoOOH, and (C) I^-. (D) The etching time of Au NBPs. (The concentration of β-Gal is 10.0 U/L.) Error bars show standard deviations of the three repeated experiments.

Note: The β-Gal standard sample at 10.0 U/L was employed to optimize the analytical conditions including the concentrations of PAPG substrates, CoOOH, I^-, and the etching time of Au NBPs. As displayed from Fig. S9, the optimized concentrations of PAPG substrates, CoOOH, and I^- are 0.5 mM, 20 μg/mL, and 1.5 mM, respectively.

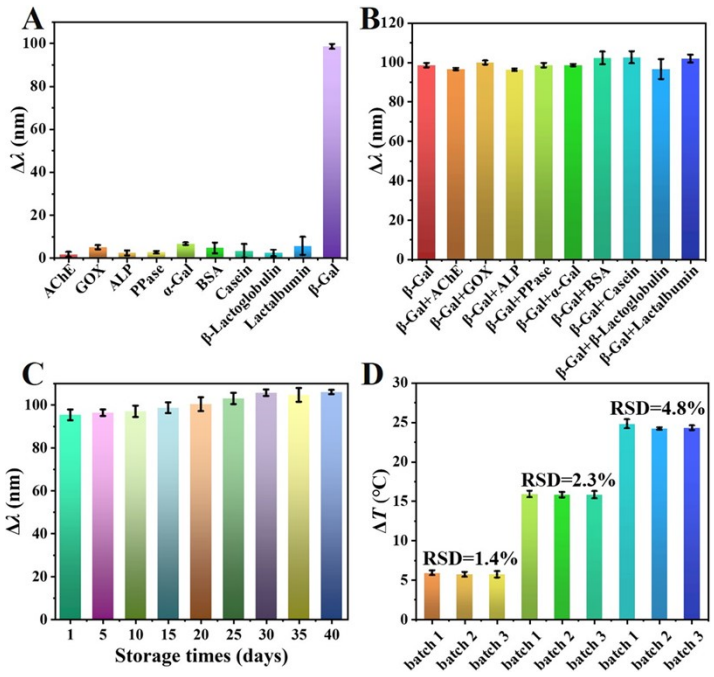

Fig. S10. Analytical performances of this proposed dual-mode biosensing methods for detecting β-Gal activities. Investigations of (A) selectivity and (B) anti-interference capability (note: β-Gal activity is 10.0 U/L, and the other interferences are 100 U/L.), (C) stability, and (D) reproducibility. Error bars indicate the standard deviations of the three repeated experiments.

Note: At first, the β-Gal (10.0 U/L) as target, and acetylcholinesterase (AChE), glucose oxidase (GOX), alkaline phosphatase (ALP), pyrophosphatase (PPase), and α-galactosidase (α-Gal) as interferences (100.0 U/L) were used to validate the specificity of this proposed sensor. As seen from Fig. S10A, comparing with the above interferences, the presence of β-Gal (10.0 U/L) in sensing system caused the wavelength shift variations (Δλ) of about 95~100 nm (Fig. S10B). The introduction of the other interferences in β-Gal systems also couldn't affect the variations of Δλ. It is demonstrated that this proposed method presented good selectivity and specificity. In this work, the as-fabricated Au NBPs, and CoOOH NRs were stored at 4 °C. Within 40 days, the Au NBPs, and CoOOH NRs were used to detect β-Gal at the 1st, 5th, 10th, 15th, 20th, 25th, 30th, 35th, and 40th day, which also exhibited stable Δλ values (Fig. S10C). It is demonstrated that this biosensor could also presented stability. Additionally, the different bathes of Au NBPs, and CoOOH NRs were detect three different activities of β-Gal (1.0, 10.0, and 100.0 U/L), respectively. As shown in Fig. S10D, the temperature variation values of ΔT approximately kept constant under the same β-Gal

activities with a relative standard deviation (RSD) of 1.4% (1.0 U/L), 2.3 % (10.0 U/L), and 4.8 % (100.0 U/L), respectively, indicating the good reproducibility of this biosensor.

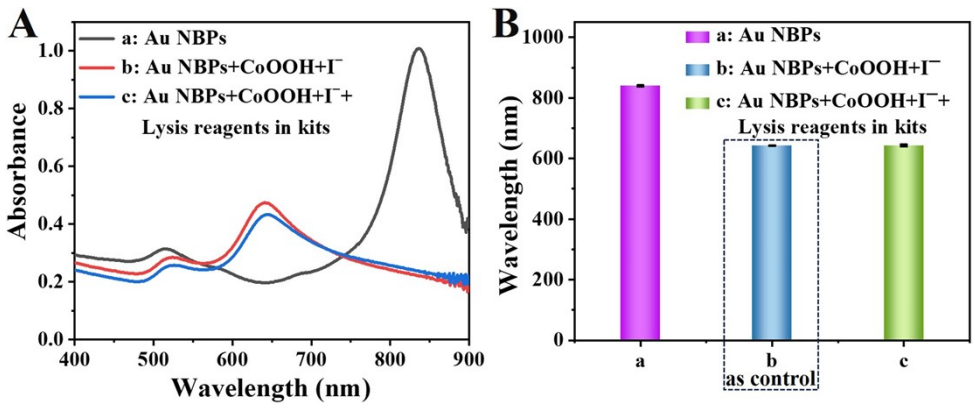

Fig. S11. Investigation of the lysis reagents in bacterial extraction kits. (A) UV-Vis spectra of (a) Au NBPs, (b) Au NBPs + CoOOH + I^-, and (c) Au NBPs + CoOOH + I^- + lysis reagents from kits. (B) Histogram statistics of the longitudinal LSPR absorption peak of Au NBPs from (A). Error bars show standard deviations of the three repeated experiments.

Note: From Fig. S11, it is demonstrated that the lysis reagents in commercial bacterial extraction kits didn't affect the shift of longitudinal LSPR absorption peak of Au NBPs.

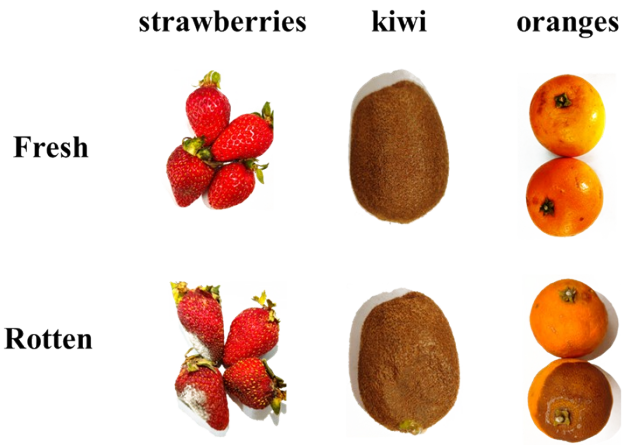

Fig. S12. Preparation of the real samples: fresh fruits and rotten fruits for the analysis of β-Gal. These fruits include the strawberries, kiwi, and oranges, which were purchased from a local supermarket.

Note: *β*-Gal is widely present in various fruits and organisms. Many works have reported that the *β*-Gal activities could be used as a marker for disease patients, and positively relate to fruit ripening.[4, 5] Therefore, in this work, the activity of *β*-Gal in rotten fruits were measured to validate the practicability of this proposed dual-mode biosensor.

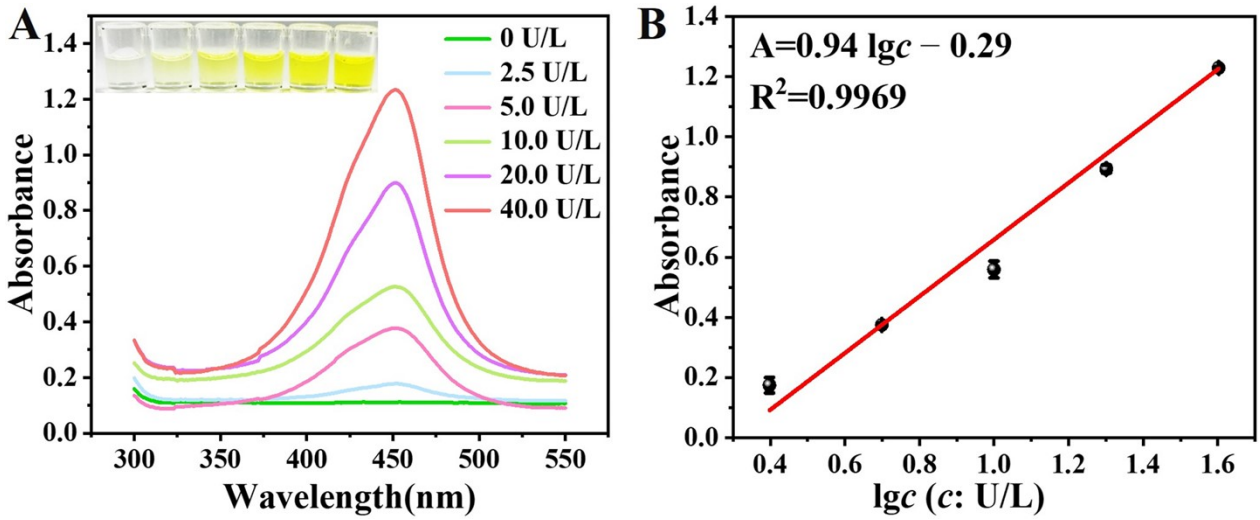

Fig. S13. *β*-Gal analysis using ELISA kits. (A) UV-Vis spectra of commercial ELISA kits response to the different concentrations of β-Gal ($c_{β\text{-Gal}}$: 0, 2.5, 5.0, 10.0, 20.0, 40.0 U/L). The inset is a colorimetric photograph for the visual analysis of β-Gal analysis. The concentrations from left to right are 0 — 40.0 U/L. (B) Calibration curve obtained by plotting absorbance (*A*) against the logarithm of the β-Gal concentrations (2.5—40.0 U/L).

Table S1. Comparisons of β-Gal analysis by using the proposed dual-mode methods in this work and standard method (commercial ELISA kits).

Samples	Types of fruits	This work (LSPR-based method)		This work (Photothermal method)		Commercial ELISA kits	
		Found (U/L)	RSD (%, *n* = 3)	Found (U/L)	RSD (%, *n* = 3)	Found (U/L)	RSD (%, *n* = 3)
Fresh fruits	Oranges	No found	–	–	–	–	–
	Kiwi	No found	–	–	–	–	–
	Strawberries	No found	–	–	–	–	–
Long-term storage of rotten fruits (Stored for 20 days)	Oranges	4.52 ± 0.09	1.89	4.65 ± 0.18	3.85	4.56 ± 0.11	2.38
	Kiwi	4.99 ± 0.10	1.89	5.14 ± 0.20	3.85	5.17 ± 0.13	2.45
	Strawberries	4.05 ± 0.15	3.77	4.23 ± 0.11	2.54	4.27 ± 0.19	4.50

Table S2. Detection of *E. Coli* in real food sample (aseptic milk) by the proposed POCT method in this work. The aseptic milk were placed in different stored environments.[a]

Samples	This work (LSPR-based method)		This work (Photothermal method)	
	Found (U/L)	RSD (%, n = 3)	Found (U/L)	RSD (%, n = 3)
Newly opened aseptic milk	No found	–	No found	–
Rest of aseptic milk stored at 37 °C for 24 h	3055 ± 102	3.34	3015 ± 132	4.37
***E. coli*-infected aseptic milk**	10798 ± 367	3.40	14580 ± 638	4.38

[a] **The aseptic milk were purchased from a local supermarket. No bacteria were detected in the newly opened milk.**

Table S3 Comparison between the dual-mode biosensing platform for β-Gal activity analysis in this work and other detection methods.

Detection methods	Linear range	Detection limit	References
Semiconducting polymer nanoparticles-based near-infrared fluorescent analysis	0 – 0.120 U/mL	0.046 U/mL	6
AIE fluorescent analysis	0 – 10 U/mL	0.22 U/mL	7
Copper nanoclusters-based luminescent sensors	3.3 – 19.7 U/L	0.45 U/L	8
Cu/N co-doped carbon-based nanozyme cascade reaction biosensor	0.025 – 0.2 U/mL	0.01 U/mL	9
Hierarchical Self-Assembly Molecular Building Blocks as Intelligent Nanoplatforms	2 – 30 U/L	0.5 U/L	10
$CoOOH/I_2$-mediated colorimetric and photothermal dual-mode biosensors	0.5 – 300 U/L (Colorimetric analysis) 0.5 – 200 U/L (Photothermal analysis)	0.43 U/L (Colorimetric analysis) 0.46 U/L (Photothermal analysis)	This work

Table S4 Comparison between the dual-mode biosensing platform based on *β*-Gal for *E. coli* activity analysis in this work and other analytical methods.

Detection methods	Linear range (CFU/mL)	Detection limit (CFU/mL)	References
Self-assembled β-galactosidase on T4 phage capsid-mediated *E. coli* detection	7.2×10^3 – 7.2×10^7	7.2×10^3	11
Permeabilization-free β-galactosidase-induction-based electrochemical detection	None	~ 2×10^3	12
$NaBiF_4$ upconversion nanoparticle-based electrochemiluminescent biosensor	200 – 1.0×10^5	138	13
Colorimetric sensor based on β-Galactosidase-triggered Si nanoparticles	1×10^2 – 5×10^5	100	14
Fluorescent sensor based on β-Galactosidase-triggered Si nanoparticles	1×10^2 – 1×10^4		
$CoOOH/I_2$-mediated colorimetric and photothermal dual-mode biosensors	200 – 1.0×10^7 (Colorimetric analysis) 2000 – 1.0×10^7 (Photothermal analysis)	182 (Colorimetric analysis) 211 (Photothermal analysis)	This work

References

1. D. Y. Li, L. Chen, C. Y. Li, J. Zhang, Y. Zhao, Y. H. Yang and T. Yang, *Biosens. Bioelectron.*, 2024, **247**, 115912.
2. Y. Wang, A. Tu, X. Zhang, M. Li, L. Liu, Y. Li, J. Wu and P. Zhang, *Chem. Eng. J.*, 2021, **426**, 131834.
3. L. Wang, T. Li, X. Dong, M. Pang, S. Xiao and W. Zhang, *Chem. Eng. J.*, 2021, **425**, 130578.
4. S. Chen, X. Ma, L. Wang, Y. Wu, Y. Wang, S. Hou and W. Fan, *Sens. Actuators, B*, 2023, **387**, 133787.
5. Y.-M. Shan, K.-K. Yu, F.-Y. Yu, Y.-H. Liu, X.-Q. Yu and K. Li, *Food Chem.*, 2024, **431**, 137117.
6. Y. Zhao, S. Sun, Y. Lyu, M. Gao, H. Lin and C. Yang, *Chem. Commun.*, 2023, **59**, 2974-2977.
7. S. Zhang, X. Wang, X. Wang, T. Wang, W. Liao, Y. Yuan, G. Chen and X. Jia, *Anal. Chim. Acta*, 2022, **1198**, 339554.
8. Y. Chang, J. Wang, H. Guo, W. Yao, H. Xie, L. Li and X. Liu, *Microchim. Acta*, 2024, **191**, 768.
9. X. Zhou, M. Wang, J. Chen and X. Su, *Talanta*, 2022, **245**, 123451.
10. S. Li, Q. Chen, Q. Xu, Z. Wei, Y. Shen, H. Wang, H. Cai, M. Gu and Y. Xiao, *Adv. Sci.*, 2024, **11**, 2309547.
11. J. Xu, Q. Yang, P. Wang, D. Wu, X. Yang, W. Chen, S. Gao and S. Wang, *Sens. Actuators, B*, 2022, **359**, 131569.
12. J. Kwon, H. Y. Kang and H. Yang, *Sens. Actuators, B*, 2021, **337**, 129768.
13. D. Liu, X. Lv, C. Zhao, J. Li, J. Huang, L. Weng, L. He and S. Liu, *RSC Adv.*, 2022, **12**, 30174-30180.
14. D. Zhao, Y. Jiao, C. Zhang and X. Xiao, *Food Chem.*, 2024, **450**, 139331.